

Enhancing AGN efficiency and cool-core formation with anisotropic thermal conduction

David J. Barnes¹^{*}, Rahul Kannan²[†], Mark Vogelsberger¹[‡], Christoph Pfrommer³,
Ewald Puchwein^{4,5}, Rainer Weinberger⁶, Volker Springel^{6,7,8}, Rüdiger Pakmor⁶,
Dylan Nelson⁸, Federico Marinacci^{1,2}, Annalisa Pillepich⁹, Paul Torrey¹, Lars Hernquist²

¹*Department of Physics, Kavli Institute for Astrophysics and Space Research, Massachusetts Institute of Technology, Cambridge, MA 02139, USA*

²*Harvard–Smithsonian Center for Astrophysics, 60 Garden Street, Cambridge, MA 02138*

³*Leibniz-Institut für Astrophysik Potsdam (AIP), An der Sternwarte 16, 14482 Potsdam, Germany*

⁴*Institute of Astronomy, University of Cambridge, Madingley Road, Cambridge, CB3 0HA, UK*

⁵*Kavli Institute for Cosmology, University of Cambridge, Madingley Road, Cambridge CB3 0HA, UK*

⁶*Heidelberg Institute for Theoretical Studies, Schloss-Wolfsbrunnengasse 35, D-69118 Heidelberg, Germany*

⁷*Zentrum für Astronomie der Universität Heidelberg, ARI, Mönchhofstr. 12-14, D-69120 Heidelberg, Germany*

⁸*Max-Planck-Institut für Astrophysik, Karl-Schwarzschild-Str. 1, 85741 Garching, Germany*

⁹*Max-Planck-Institut für Astronomie, Königstuhl 17, 69117 Heidelberg, Germany*

Accepted XXX. Received YYY; in original form ZZZ

ABSTRACT

Understanding how baryonic processes shape the intracluster medium (ICM) is of critical importance to the next generation of galaxy cluster surveys. However, most models of structure formation neglect potentially important physical processes, like anisotropic thermal conduction (ATC). In this letter, we explore the impact of ATC on the prevalence of cool-cores (CCs) using 12 pairs of magnetohydrodynamical galaxy cluster simulations, simulated using the IllustrisTNG model with and without ATC. Although the impact of ATC varies from cluster to cluster and with CC criterion, its inclusion produces a systematic shift to larger CC fractions at $z = 0$ for all CC criteria considered. Additionally, the inclusion of ATC yields a flatter CC fraction redshift evolution, easing the tension with the observed evolution. With ATC included, the energy required for the central black hole to achieve self-regulation is reduced and the gas fraction in the cluster core increases, resulting in larger CC fractions. ATC makes the ICM unstable to perturbations and the increased efficiency of AGN feedback suggests that its inclusion results in a greater level of mixing in the ICM. Therefore, ATC is potentially an important physical process in reproducing the thermal structure of the ICM.

Key words: galaxies: clusters: general – galaxies: clusters: intracluster medium – conduction – methods: numerical

1 INTRODUCTION

The thermal structure of the hot gas that fills galaxy clusters, the intracluster medium (ICM), is very sensitive to the baryonic processes that are ongoing within the cluster volume. Cooling, heat transport, turbulence, plasma physics, cosmic rays, magnetic fields and energy injection from supernovae and active galactic nuclei (AGN) all combine to shape the ICM and its observable properties. A thermal structure common to many galaxy clusters is a cool core (CC). This is a cold, dense central core whose X-ray emission implies a cooling time shorter than the age of the Universe (e.g. Lewis et al. 2002; Peterson et al. 2003) and is often associated with

a relaxed morphology. Recent observations have shown that CCs exist at high-redshift ($z > 1$) and that their properties appear to be roughly independent of redshift (McDonald et al. 2017).

Reproducing CCs in cosmological galaxy cluster simulations remains a significant challenge. Even recent numerical work with subgrid prescriptions that include feedback from AGN struggle to reproduce the observed CC fractions from unbiased, low-redshift samples. The exact level of agreement with the observations depends on the chosen CC criteria (e.g. Hudson et al. 2010) and the simulated samples are small ($\sim 10 - 30$ objects), due to their computational expense (e.g. Rasia et al. 2015; Hahn et al. 2017), limiting any statistically meaningful comparison. Barnes et al. (2017a) recently explored six common CC criteria using clusters from the TNG300 volume of IllustrisTNG, which provided a sample of 370 clusters at $z = 0$. They found that the IllustrisTNG model yields reasonable agreement for some criteria compared to observed low-

^{*} E-mail: djbarnes@mit.edu

[†] Einstein Fellow

[‡] Alfred P. Sloan Fellow

redshift observations, although the evolution of the CC fraction with redshift was found to be steeper than the observed trend.

However, even state-of-the-art cluster formation simulations include only the minimum physical processes required to reproduce an ICM that has reasonable global properties (e.g. [Rasia et al. 2015](#); [McCarthy et al. 2017](#); [Barnes et al. 2017b](#); [Henden et al. 2018](#)), i.e. cooling, star formation and feedback from supernovae and AGN. The vast majority neglect important physical processes known to impact the thermal properties of the ICM, like magnetic fields (e.g. [Carilli & Taylor 2002](#)), cosmic rays (e.g. [Pfrommer 2013](#); [Ruszkowski et al. 2017](#); [Jacob & Pfrommer 2017](#)) and thermal conduction (e.g. [Quataert 2008](#); [Sharma et al. 2009](#)). The exact impact of thermal conduction in the ICM is still unclear, the strong temperature dependence of the heat flux ($Q \propto T^{7/2}$) requires the conductivity to be fine tuned ([Zakamska & Narayan 2003](#)) and the solutions are only locally stable on scales of the field length ([Soker 2003](#)). Though thermal conduction is likely not capable of completely offsetting radiative losses, it may provide part of the heating required and it makes the ICM unstable to instabilities in the presence of external turbulence ([Sharma et al. 2009](#); [Banerjee & Sharma 2014](#)). In a magnetized, weakly collisional plasma, such as the ICM, anisotropic thermal conduction (ATC) is the relevant heat transport process, with heat transport perpendicular to the magnetic field suppressed. For a single cluster, [Kannan et al. \(2017\)](#) demonstrated that ATC led to increased mixing and AGN feedback being more efficiently coupled to the ICM, reducing the overall energy input while increasing its ability to quench star formation.

In this Letter, we explore the impact of ATC on the formation and maintenance of CCs via cosmological zoom simulations of galaxy clusters and demonstrate that difference can be linked to efficiency with which AGN feedback couples to the ICM.

2 NUMERICAL METHOD

In this work we use 12 galaxy clusters from the AESTUS simulation suite ([Kannan et al. in prep.](#)) covering the mass range $1.0 \times 10^{14} M_{\odot} < M_{500} < 2.7 \times 10^{15} M_{\odot}$. The suite consists of zoom simulations of galaxy clusters extracted from the Millennium XXL simulation ([Angulo et al. 2012](#)), with cosmological parameters rescaled to the measurements of [Planck Collaboration et al. \(2016\)](#): $\Omega_M = 0.3089$, $\Omega_{\Lambda} = 0.6911$, $\Omega_b = 0.0486$, $\sigma_8 = 0.8159$, $n_s = 0.9667$ and $H = 100 h \text{ km s}^{-1} \text{ Mpc}^{-1}$ with $h = 0.6774$. The high resolution region has a dark matter and initial gas mass resolution of $5.9 \times 10^7 M_{\odot}$ and $1.1 \times 10^7 M_{\odot}$, respectively. Collisionless particles, i.e. stars and dark matter, have a softening length of 1.48 kpc that is comoving for $z > 1$ and a fixed physical length for $z \leq 1$. The gas cells employ an adaptive co-moving softening length, reaching a minimum of 0.37 kpc.

The simulations employ the IllustrisTNG galaxy formation model ([Weinberger et al. 2017b](#); [Pillepich et al. 2018a](#)), an updated version of the Illustris model ([Vogelsberger et al. 2013](#); [Torrey et al. 2014](#); [Vogelsberger et al. 2014b,a](#); [Genel et al. 2014](#); [Sijacki et al. 2015](#)), that includes radiative cooling, star formation, metal enrichment, magnetic fields and feedback from supernovae and AGN. Initial results were presented in [Marinacci et al. \(2017\)](#), [Springel et al. \(2018\)](#), [Nelson et al. \(2018\)](#), [Pillepich et al. \(2018b\)](#), and [Naiman et al. \(2018\)](#). The metal distribution in the ICM is well matched to observed clusters ([Vogelsberger et al. 2018](#)). A census of the CC clusters in the TNG300 volume and the redshift evolution of the CC fraction was presented in [Barnes et al. \(2017a\)](#).

Each cluster in the suite is run twice, a fiducial run and a run that additionally includes ATC. The numerical implementation of ATC follows the approach introduced in [Kannan et al. \(2016\)](#). The

Table 1. Table summarizing the CC criteria used in this work.

Criterion	Notation	CC limit
Central electron number density	n_e	$> 1.5 \times 10^{-2} \text{ cm}^{-3}$
Central cooling time	t_{cool}	$< 1 \text{ Gyr}$
Central entropy excess	K_0	$< 30 \text{ keV cm}^{-2}$
Concentration parameter (physical)	C_{phys}	> 0.155
Concentration parameter (scaled)	C_{scal}	> 0.5
Cuspidity parameter	α	> 0.75

value of the conduction coefficient is set to the canonical Spitzer value ([Spitzer 1962](#)) parallel to the magnetic field, with a maximum diffusive value of $5 \times 10^{31} \text{ cm}^2 \text{ s}^{-1}$ ([Ruszkowski et al. 2011](#); [Yang & Reynolds 2016](#)), and zero in the direction perpendicular to the field. The conduction routine is not active for star-forming gas cells that follow an imposed equation of state ([Springel & Hernquist 2003](#)). This conduction coefficient value is likely optimistic, as plasma effects, like mirror instabilities ([Komarov et al. 2016](#)) and Whistler waves ([Robberg-Clark et al. 2016](#)), potentially lead to a substantial suppression of thermal conduction. However, we set the coefficient to the canonical Spitzer value to examine the maximum impact on the thermal structure of the ICM. [Gaspari & Churazov \(2013\)](#) have previously argued that the conduction coefficient in the ICM for isotropic conduction is negligible, however isotropic conduction is incorrect in the presence of a magnetized plasma and the value of the conduction coefficient in the ICM is still unclear.

3 CC FRACTIONS AND REDSHIFT EVOLUTION

The CC definitions used in this work are summarized in Table 1 and we refer the interested reader to [Barnes et al. \(2017a\)](#) for a thorough description of how these criteria are calculated.

In the main panels of Fig. 1 we present the CC criteria as a function of M_{500} at $z = 0$. For a matched pair of clusters the impact of ATC varies, with several clusters showing large shifts towards the CC tail of the criterion distribution and two clusters producing small shifts towards the non-cool-core (NCC) tail. The change induced on a matched pair by ATC also varies from criterion to criterion. However, for all CC criteria explored in this work the inclusion of ATC leads to a systematic shift in the distributions towards larger CC fractions, as shown in the side panels. The fractional changes in the median CC criteria values relative to without ATC are $\Delta n_e/n_e = 0.28$, $\Delta t_{\text{cool}}/t_{\text{cool}} = -0.43$, $\Delta K_0/K_0 = -0.50$, $\Delta C_{\text{phys}}/C_{\text{phys}} = 0.62$, $\Delta C_{\text{scal}}/C_{\text{scal}} = 0.22$, $\Delta \alpha/\alpha = 0.51$. The heat flux has a strong temperature dependence, $Q \propto T^{7/2}$, and we split the clusters by M_{500} to explore this, with the 6 most massive clusters forming a hotter sample and 6 least massive forming a cooler sample. The inclusion of ATC produces a greater difference in the median CC criteria values of the hotter sample, with $\Delta n_e/n_e = 0.51$, $\Delta t_{\text{cool}}/t_{\text{cool}} = -0.46$, $\Delta K_0/K_0 = -0.54$, $\Delta C_{\text{phys}}/C_{\text{phys}} = 2.10$, $\Delta C_{\text{scal}}/C_{\text{scal}} = 0.32$, $\Delta \alpha/\alpha = 1.06$, compared to the cooler sample, $\Delta n_e/n_e = 0.24$, $\Delta t_{\text{cool}}/t_{\text{cool}} = -0.41$, $\Delta K_0/K_0 = -0.48$, $\Delta C_{\text{phys}}/C_{\text{phys}} = 0.30$, $\Delta C_{\text{scal}}/C_{\text{scal}} = 0.14$, $\Delta \alpha/\alpha = 0.41$.

To further explore the shift to larger CC fractions when ATC is included, we plot the mean cumulative gas fraction radial profiles at $z = 0$ for clusters with and without ATC in Fig. 2. We note that the shape of the gas fraction profile is inconsistent with the shape of the observed profile ([Pratt et al. 2010](#)). The inclusion of ATC leads to an increased average gas fraction throughout the cluster volume, but the difference reduces at larger radii. The fractional difference at r_{500} is only a 1 per cent increase when ATC is included, however

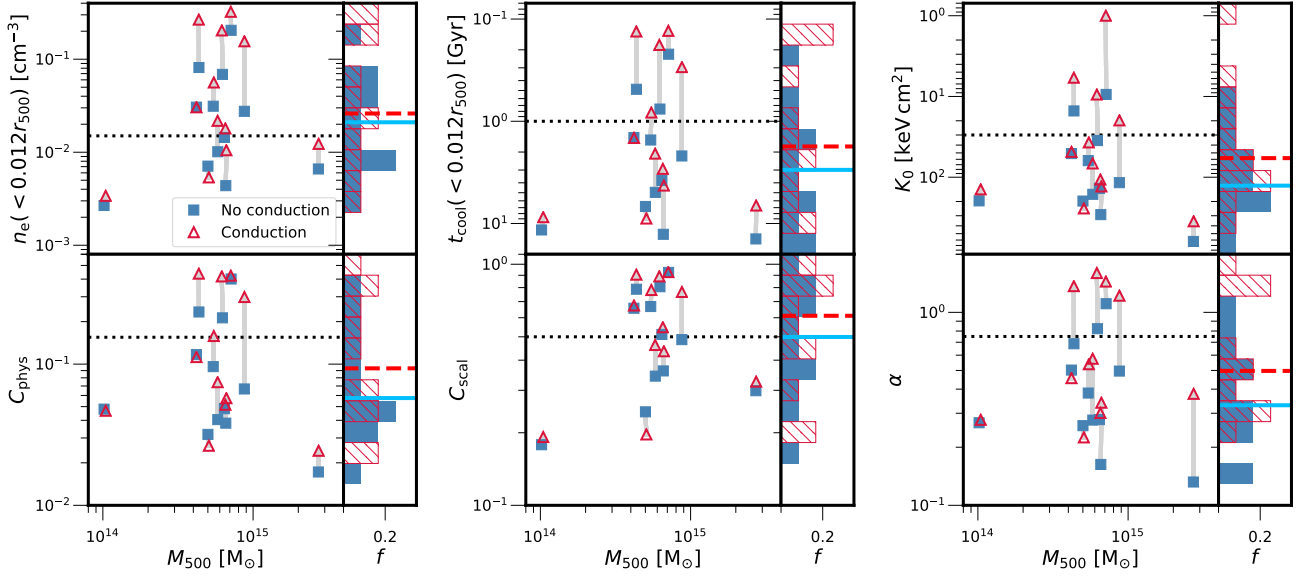


Figure 1. Six different CC criteria at $z = 0$ for the clusters run with (red triangle) and without (blue square) anisotropic thermal conduction. Grey lines link matched clusters with the dotted black line denoting the CC threshold. We note the y-axis is inverted for the cooling time and central entropy excess. In the side panels the criteria distributions with (red hashed) and without (solid blue) are shown, with the median of the distributions denoted by the red dashed and blue solid lines, respectively. The inclusion of anisotropic thermal conduction produces a systematic shift towards larger CC fractions.

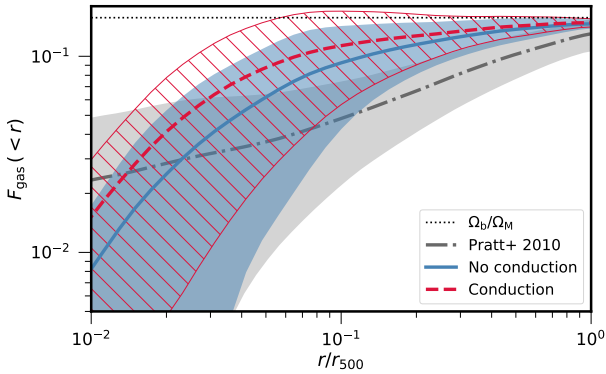


Figure 2. Cumulative mean gas fraction profile at $z = 0$ with (red dashed) and without (blue solid) ATC. The shaded region denotes one standard deviation of the sample. The mean observed gas fraction profile (grey dash-dot) and associated standard deviation are from the REXCESS cluster sample (Pratt et al. 2010). The inclusion leads to an increased gas fraction throughout the cluster volume, but especially in the cores of clusters defined as CC.

at $0.01r_{500}$, its inclusion yields a 100 per cent increase in the gas fraction. In addition, the inclusion of ATC leads to an increase in the scatter of the gas fraction profiles, with some profiles exceeding the universal baryon fraction (Ω_b/Ω_M) at $0.1r_{500}$. Defining CCs by the central electron number density criterion, all of these systems are defined as CCs. In contrast, the cumulative gas fraction profiles of NCC systems remain relatively unchanged with the inclusion of ATC.

The systematically higher gas fractions at $0.01r_{500}$ with the inclusion of ATC will result in increased central electron number densities, shifting the distribution to a greater fraction of CCs for a fixed density threshold. With $t_{\text{cool}} \propto n_e^{-1}$ and $K \propto n_e^{-2/3}$, the increased central density will result in a shorter cooling time and a lower central entropy excess, which for a population of clusters will result in higher CC fractions. Finally, higher central densities will increase the X-ray emission from cluster cores, due to its n_e^2

dependence, and result in larger concentration parameter values and more clusters being defined as CCs.

Since the CC fraction for all 6 criteria increased at $z = 0$ with the introduction of ATC, we now explore its impact on the CC fraction as a function of redshift. For all six criteria we calculate the CC fraction between $z = 2$ and $z = 0$, estimating the 1σ confidence intervals via the beta distribution quantile technique (Cameron 2011), and then estimate the redshift evolution by fitting a linear relation that accounts for the uncertainties. We perform this fit for both samples, with and without ATC, and the difference between them is shown in the main panel of Fig. 3. The addition of ATC yields the same trend for all six criteria, a reduction in the CC fraction at high-redshift ($z > 1$) and an increase in the CC fraction at low-redshift. The exact change is dependent on the selected criterion, with the scaled concentration parameter showing the smallest reduction at $z = 2$ ($\Delta f_{\text{CC}} = -0.06$) and one of the largest increases in CC fraction at $z = 0$ ($\Delta f_{\text{CC}} = 0.17$). The central entropy excess has the shallowest change between $z = 2$ and $z = 0$, and the smallest increase in the CC fraction at low-redshift. Barnes et al. (2017a) demonstrated that in general the IllustrisTNG model underproduced CCs at low-redshift and overproduced them at high-redshift. In the inset of Fig. 3 we demonstrate that applying the correction factor to the redshift evolution found for such a statistically large sample, specifically the high mass ($M_{500} > 2 \times 10^{14} M_\odot$) IllustrisTNG sample, eases tension with the observed redshift evolution trend for the central cooling time criterion. The observations are taken from Cavagnolo et al. (2009, C+09) and McDonald et al. (2013, McD+13). For all criteria the addition of ATC would ease the tension with the observed redshift evolution, even if the normalization of the CC fraction still differs from observations.

4 THE LINK TO AGN EFFICIENCY

The inclusion of ATC yields an increased CC fraction, an increased central cumulative gas fraction and a flattened redshift evolution of the CC fraction. To further understand these changes we examine the energy injected by the AGN and its coupling to the ICM. For

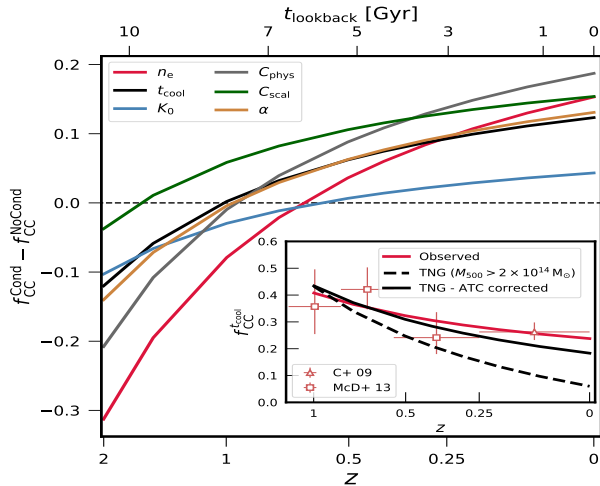


Figure 3. CC fraction difference with and without ATC as a function of redshift, for the central electron number density (red), cooling time (black), central entropy excess (blue), physical (grey) and scaled (green) concentration parameters and the cuspsiness parameter (yellow). *Inset:* Defining CCs by the central cooling time criterion, the correction factor eases the tension with the observed evolution (Cavagnolo et al. 2009; McDonald et al. 2013) for the IllustrisTNG high-mass sample (Barnes et al. 2017a).

each cluster the central black hole is defined as the most massive black hole within 1 kpc of the potential minimum at $z = 0$ and we then traced its properties as a function of redshift. At late times the kinetic mode feedback dominates (Weinberger et al. 2017a), and the left panel of Fig. 4 shows the median energy injected by the kinetic mode as a function of redshift, with and without ATC. At $z = 0$, the inclusion of ATC results in a 24 per cent reduction in the energy injected by the low accretion rate kinetic feedback mode. The right axis shows central black hole mass and the central galaxy stellar mass, defined as the mass within twice the stellar half-mass radius of the main halo defined by SUBFIND, and the inclusion of ATC produces negligible change in both.

As an AGN will continue to inject energy until it is able to self-regulate, the lack of change in black hole or central galaxy mass and the reduction in the energy injected for simulations with ATC suggests that ATC increases the efficiency with which feedback couples to the surrounding ICM. In this work, the AGN efficiency, ε , is defined as the ratio of the total cumulative energy lost by the ICM via radiative cooling over the cumulative energy injected by the central AGN. When calculating the cumulative energy lost via cooling we only consider non-star-forming gas that is cooling, i.e. not being heated by supernovae or AGN feedback, and has a temperature $T \geq 10^6$ K. Between $z = 2$ and $z = 0$ the cluster collapses and grows substantially and so the energy lost via cooling is measured inside spherical apertures scaled by r_{500} : $0.15r_{500}$ and $1.0r_{500}$. The median AGN efficiency is plotted in the central panel of Fig. 4. Regardless of the inclusion ATC, AGN efficiency decreases towards low redshift, reducing by a factor of ~ 5 between $z = 2$ and $z = 0$ for both apertures. This increased efficiency at high redshift is a combination of the AGN injecting less energy, which is seen by the steeper than linear increase in cumulative injected energy, and the increasing critical density of the Universe with redshift, which results in shorter gas cooling times (due to its $1/n$ dependence) and greater energy loss.

Finally, in the right panel of Fig. 4 we plot the fractional difference between the median AGN efficiency of the simulations with and without ATC inside apertures of $0.15r_{500}$ and $1.0r_{500}$.

For $z > 0.75$ the two sets of simulations have very similar AGN efficiencies within all apertures, but there is some evidence that at very high redshift ($z > 1.5$) the inclusion of ATC leads to a lower AGN efficiency. For $z < 0.75$ there is a clear difference in the AGN efficiencies, with the inclusion of ATC yielding a ~ 50 per cent increase in AGN efficiency compared to the simulations without it. This difference appears to be a function of aperture size, with the smaller aperture ($0.15r_{500}$) producing a greater difference in efficiencies compared to the larger aperture, though it is noisy.

The introduction of ATC fundamentally changes the response of the ICM to perturbations, such as AGN feedback. If a temperature gradient is present then it is unstable either to the heat-flux-driven buoyancy instability (Quataert 2008) or to the magnetothermal instability (Balbus 2000), and any external perturbation will result in the plasma mixing (Sharma et al. 2009). Kannan et al. (2017) have already, for a single cluster, shown that the inclusion of ATC results in a greater level of mixing. The increased coupling efficiency of the AGN feedback suggests that ATC is enhancing the mixing in the ICM, distributing the kinetic mode feedback more isotropically. This requires less energy per unit time to be injected by the central black hole to offset radiative losses, which softens the AGN feedback and increases the central gas density and the measured CC fraction.

5 CONCLUSIONS

We have examined the impact of ATC on CC formation and AGN feedback efficiency using 12 zoom cosmological MHD galaxy cluster simulations. Each cluster was run with and without ATC using the IllustrisTNG model. ATC was self-consistently included following the method of Kannan et al. (2016). Our main results are:

- Although the impact of ATC varied on a cluster by cluster and on a CC criterion basis, its inclusion produced a systematic shift of all criteria distributions to larger CC fractions (Fig. 1). This is the result of an increased central gas fraction with ATC (Fig. 2).
- Exploring the redshift evolution of the CC fraction, we found that inclusion of ATC resulted in a decreased CC fraction at high redshift ($z \geq 1$) and an increased CC fraction at low redshift ($z < 1$) (Fig. 3). For the statistically large sample produced by IllustrisTNG (Barnes et al. 2017a), the correction due to ATC would ease the tension between the simulated and observed redshift evolution of the CC fraction.
- Finally, we examined the total energy injected by the central black hole and found that inclusion of ATC resulted in a 7 per cent decrease in the total energy injected, due to the kinetic feedback mode injecting 24 per cent less energy during the formation of the cluster (Fig. 4). The increased efficiency of AGN feedback suggests that ATC increases the mixing in the ICM, softening the impact of AGN feedback and producing higher central gas fractions.

The results suggest that the inclusion of ATC alters the response of the ICM to AGN feedback, making it unstable to convective mixing in the presence of external perturbations. The increased mixing makes the AGN-ICM coupling more efficient, reducing the energy required for self-regulation (e.g. Kannan et al. 2017). This results in increased low-redshift CC fractions and flatter redshift evolution compared to the same model without ATC. Previous numerical work with artificial thermal conduction that promoted mixing also found an improved match to observed CC fractions (Rasia et al. 2015). The inclusion of ATC reduces the entropy injected by a self-regulating black hole, suggesting its inclusion may help numerical simulations reproduce the thermal structure of cluster cores.

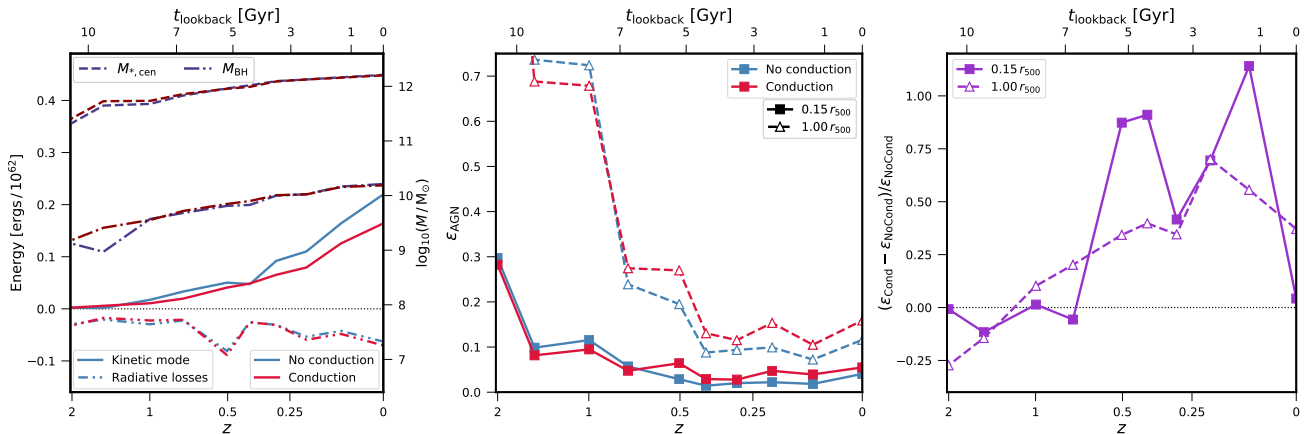


Figure 4. AGN feedback efficiency with (red) and without (blue) anisotropic thermal conduction. *Left:* Median cumulative energy injected in the kinetic mode (solid) as a function of redshift by the black hole compared to the radiative losses within r_{500} (dash-dotted). Median stellar mass of the central galaxy (dashed) and black hole mass (dash-dot) are shown by the right scale. *Centre:* AGN efficiency, ϵ , measured as the ratio of radiative losses to total energy injected, as a function of redshift within apertures of $0.15r_{500}$ (solid) and $1.0r_{500}$ (dashed). *Right:* Fractional difference in median AGN efficiency between simulations with and without thermal conduction. Anisotropic thermal conduction results in less energy being injected by the AGN, but a more efficient AGN-ICM coupling.

ACKNOWLEDGEMENTS

The simulations were performed on the MKI-Harvard Odyssey cluster and the Stampede supercomputers at the Texas Advanced Computing Center as part of XSEDE project TG-AST160069. RK acknowledges support from NASA through Einstein Postdoctoral Fellowship grant number PF7-180163 awarded by the *Chandra* X-ray Center, which is operated by the Smithsonian Astrophysical Observatory for NASA under contract NAS8-03060. MV acknowledges support through an MIT RSC award, the support of the Alfred P. Sloan Foundation, and support by NASA ATP grant NNX17AG29G. PT acknowledges support from NASA through Hubble Fellowship grants HST-HF2-51384.001-A awarded by the STScI, which is operated by the Association of Universities for Research in Astronomy, Inc., for NASA, under contract NAS5-26555. CP acknowledges support by the European Research Council under ERC-CoG grant CRAGSMAN-646955.

REFERENCES

Angulo R. E., Springel V., White S. D. M., Jenkins A., Baugh C. M., Frenk C. S., 2012, *MNRAS*, **426**, 2046
 Balbus S. A., 2000, *ApJ*, **534**, 420
 Banerjee N., Sharma P., 2014, *MNRAS*, **443**, 687
 Barnes D. J., et al., 2017a, preprint, ([arXiv:1710.08420](https://arxiv.org/abs/1710.08420))
 Barnes D. J., et al., 2017b, *MNRAS*, **471**, 1088
 Cameron E., 2011, *Publ. Astron. Soc. Australia*, **28**, 128
 Carilli C. L., Taylor G. B., 2002, *ARA&A*, **40**, 319
 Cavagnolo K. W., Donahue M., Voit G. M., Sun M., 2009, *ApJS*, **182**, 12
 Gaspari M., Churazov E., 2013, *A&A*, **559**, A78
 Genel S., et al., 2014, *MNRAS*, **445**, 175
 Hahn O., Martizzi D., Wu H.-Y., Evrard A. E., Teyssier R., Wechsler R. H., 2017, *MNRAS*, **470**, 166
 Henden N. A., Puchwein E., Shen S., Sijacki D., 2018, preprint, ([arXiv:1804.05064](https://arxiv.org/abs/1804.05064))
 Hudson D. S., Mittal R., Reiprich T. H., Nulsen P. E. J., Andernach H., Sarazin C. L., 2010, *A&A*, **513**, A37
 Jacob S., Pfrommer C., 2017, *MNRAS*, **467**, 1449
 Kannan R., Springel V., Pakmor R., Marinacci F., Vogelsberger M., 2016, *MNRAS*, **458**, 410
 Kannan R., Vogelsberger M., Pfrommer C., Weinberger R., Springel V., Hernquist L., Puchwein E., Pakmor R., 2017, *ApJ*, **837**, L18
 Komarov S. V., Churazov E. M., Kunz M. W., Schekochihin A. A., 2016, *MNRAS*, **460**, 467

Lewis A. D., Stocke J. T., Buote D. A., 2002, *ApJ*, **573**, L13
 Marinacci F., et al., 2017, preprint, ([arXiv:1707.03396](https://arxiv.org/abs/1707.03396))
 McCarthy I. G., Schaye J., Bird S., Le Brun A. M. C., 2017, *MNRAS*, **465**, 2936
 McDonald M., et al., 2013, *ApJ*, **774**, 23
 McDonald M., et al., 2017, *ApJ*, **843**, 28
 Naiman J. P., et al., 2018, *MNRAS*,
 Nelson D., et al., 2018, *MNRAS*, **475**, 624
 Peterson J. R., Kahn S. M., Paerels F. B. S., Kaastra J. S., Tamura T., Bleeker J. A. M., Ferrigno C., Jernigan J. G., 2003, *ApJ*, **590**, 207
 Pfrommer C., 2013, *ApJ*, **779**, 10
 Pillepich A., et al., 2018a, *MNRAS*, **473**, 4077
 Pillepich A., et al., 2018b, *MNRAS*, **475**, 648
 Planck Collaboration et al., 2016, *A&A*, **594**, A13
 Pratt G. W., et al., 2010, *A&A*, **511**, A85
 Quataert E., 2008, *ApJ*, **673**, 758
 Rasia E., et al., 2015, *ApJ*, **813**, L17
 Roberg-Clark G. T., Drake J. F., Reynolds C. S., Swisdak M., 2016, *ApJ*, **830**, L9
 Ruszkowski M., Lee D., Brügggen M., Parrish I., Oh S. P., 2011, *ApJ*, **740**, 81
 Ruszkowski M., Yang H.-Y. K., Reynolds C. S., 2017, *ApJ*, **844**, 13
 Sharma P., Chandran B. D. G., Quataert E., Parrish I. J., 2009, *ApJ*, **699**, 348
 Sijacki D., Vogelsberger M., Genel S., Springel V., Torrey P., Snyder G. F., Nelson D., Hernquist L., 2015, *MNRAS*, **452**, 575
 Soker N., 2003, *MNRAS*, **342**, 463
 Spitzer L., 1962, *Physics of Fully Ionized Gases*
 Springel V., Hernquist L., 2003, *MNRAS*, **339**, 289
 Springel V., et al., 2018, *MNRAS*, **475**, 676
 Torrey P., Vogelsberger M., Genel S., Sijacki D., Springel V., Hernquist L., 2014, *MNRAS*, **438**, 1985
 Vogelsberger M., Genel S., Sijacki D., Torrey P., Springel V., Hernquist L., 2013, *MNRAS*, **436**, 3031
 Vogelsberger M., et al., 2014a, *MNRAS*, **444**, 1518
 Vogelsberger M., et al., 2014b, *Nature*, **509**, 177
 Vogelsberger M., et al., 2018, *MNRAS*, **474**, 2073
 Weinberger R., et al., 2017a, preprint, ([arXiv:1710.04659](https://arxiv.org/abs/1710.04659))
 Weinberger R., et al., 2017b, *MNRAS*, **465**, 3291
 Yang H.-Y. K., Reynolds C. S., 2016, *ApJ*, **829**, 90
 Zakamska N. L., Narayan R., 2003, *ApJ*, **582**, 162

This paper has been typeset from a $\text{\TeX}/\text{\LaTeX}$ file prepared by the author.